

Electrostatic fluctuations in cavities within polar liquids and thermodynamics of polar solvation

Daniel R. Martin and Dmitry V. Matyushov

Center for Biological Physics, Arizona State University, PO Box 871604, Tempe, AZ 85287-1604

We present the results of numerical simulations of fluctuations of the electrostatic potential and electric field inside cavities created in the fluid of dipolar hard spheres. We found that the thermodynamics of polar solvation dramatically changes its regime when the cavity size becomes about 4-5 times larger than the size of the liquid particle. The range of small cavities can be reasonably understood within the framework of current solvation models. On the contrary, the regime of large cavities is characterized by a significant softening of the cavity interface resulting in a decay of the fluctuation variances with the cavity size much faster than anticipated by both the continuum electrostatics and microscopic theories. For instance, the variance of potential decays with the cavity size R_0 approximately as $1/R_0^{4-6}$ instead of the $1/R_0$ scaling expected from standard electrostatics. Our results suggest that cores of non-polar molecular assemblies in polar liquids lose solvation strength much faster than is traditionally anticipated.

PACS numbers:

I. INTRODUCTION

Solvation represents the change in the free energy when a usually molecular object is inserted into a condensed-phase environment. Since a significant part of chemistry and all life processes happen in liquid solutions, the traditional focus has been on solvation in liquids, polar liquids in particular. The heterogeneous problem of solvation is probably as complex as the theory of liquids itself and is hunted by the same basic issues making the quantitative description of liquids so hard. There are two dominating and mutually compensating contributions to the free energy of solvation: the positive free energy of creating a cavity (empty space) for a molecule to be inserted and a negative stabilization energy from short range (van der Waals) and long-range (electrostatic) forces [1]. The positive cavity free energy is normally significantly compensated by the negative stabilization free energy resulting in the overall solvation free energy, a situation akin to the competition between repulsive and attractive forces in equilibrium liquids [2].

The present study is devoted to electrostatic solvation, i.e. the free energy arising from the electrostatic interactions between the charge distribution of the solute with the charge distribution of the liquid solvent. The charge distribution within molecular solutes is often modeled by atomic partial charges efficiently used in force fields of numerical simulations. On the contrary, the charge distribution of the solvent molecules is often well represented by molecular multipoles following the well-established tradition of classical electrostatics [3] and dielectric theory [4]. Extensions to models utilizing atomic charges are also possible as used in numerical simulations [5] and interaction-site models of molecular liquids [2].

Electrostatic solvation is believed to be well-understood. Following Born [6] and Onsager [7], the problem is traditionally recast in terms of continuum electrostatics where the electrostatic free energy is sought for the solute charges inserted into a dielectric cavity.

This approach has been extensively tested against the experimental database of solvation of small ions and neutral molecules in polar molecular liquids [8]. Despite some inconsistencies, the formalism can be easily incorporated into quantum calculations and can even be quantitative once the dielectric cavity is properly parametrized.

There are however still some fundamental issues that cannot be addressed within electrostatic models. The solution of the Poisson equation in dielectric media is essentially a boundary condition problem in which the assumptions tacitly made by the material Maxwell's equations about the structure of the dielectric interface are essential for the solution. The standard electrostatics assumes abrupt discontinuity of the dipolar polarization at the dielectric surface. This boundary condition creates surface charge [4] which is ultimately responsible for the electrostatic potential within the dielectric cavity. Whether interfaces of real polar liquids [9] match the assumption of abrupt discontinuity of the bulk polarization is an open question. For instance, the electric field within a cavity in a polar liquid was found to be much different from the prediction of standard electrostatics up to the cavity size of a mesoscale dimension [10].

A new additional piece of evidence comes from studies of hydrophobic solvation essential for colloid stability, biopolymer folding, and formation of biological supramolecular structures [11, 12]. It was found that solvation of non-polar solutes changes dramatically in character at the length of about 1 nm, which is about three molecular diameters for aqueous solvation [13]. Solvation of solutes larger than this characteristic length was found to be dominated by surface effects, i.e. the structure of water at the hydrophobic interface. Weak dewetting [14, 15], i.e. a substantial decrease of the water density at the interface compared to the bulk water, was found to be a central part of solvation of large hydrophobic solutes.

Given the current interest in solvation at mesoscale [16, 17], to a large extent driven by biological applications [18], we address here the problem of electrostatic

solvation of solutes significantly larger than have been mostly studied so far. Our study is driven by the question whether the change in the solvation character established for hydrophobic solutes [11] is reflected in an equally dramatic change in the character of electrostatic solvation. The fact that the properties of a polar liquid interface are inconsistent with the assumptions of Maxwell's electrostatics [10] points to the possibility of a new solution once the size of the solute exceeds some critical dimension. This is indeed the result we report here.

We have found from numerical simulations that the scaling of the fluctuations of the electrostatic potential and electric field with the cavity radius is consistent with the expectations of electrostatics (qualitatively) and molecular solvation models (quantitatively) for small solutes, but changes dramatically at approximately the same solute/solvent size ratio as observed for hydrophobic solvation. It turns out that the core of the solute becomes non-polar with its growing size much faster than is normally anticipated. We will start with formulating the general results of the Gaussian solvation thermodynamics and discuss the outcome of computer simulations next.

II. THERMODYNAMICS OF ELECTROSTATIC SOLVATION

By definition, the chemical potential of electrostatic solvation is given by the ratio of two partition functions: the one which includes the electrostatic solute-solvent potential V_{0s} and the one which is based on the non-electrostatic solute-solvent interactions and the interactions between the solvent particles. All these latter interactions are incorporated in the Hamiltonian H_0 . The relation for μ_{0s} is then

$$e^{-\beta\mu_{0s}(\beta)} = Q(\beta)^{-1} \int e^{-\beta V_{0s} - \beta H_0} d\Gamma, \quad (1)$$

where

$$Q(\beta) = \int e^{-\beta H_0} d\Gamma. \quad (2)$$

Here, we use the subscript "0" for the solute and the subscript "s" for the solvent, $d\Gamma$ denotes integration over the system phase space, and β is the inverse temperature. Equation (1) can be conveniently re-written in terms of the product of the Boltzmann distribution of finding the solute-solvent energy $\epsilon = V_{0s}$ and the probability density $P(\epsilon, \beta)$

$$e^{-\beta\mu_{0s}(\beta)} = \int P(\epsilon, \beta) e^{-\beta\epsilon} d\epsilon, \quad (3)$$

where

$$P(\epsilon, \beta) = Q(\beta)^{-1} \int \delta(\epsilon - V_{0s}) e^{-\beta H_0} d\Gamma. \quad (4)$$

Equation (3) is exact and it states that all the thermodynamic information required to understand electrostatic solvation is contained in the distribution of fluctuations of the interaction energy $\epsilon = V_{0s}$ produced by the solvent which is actually not polarized by this potential; $V_{0s} = 0$ for the Hamiltonian H_0 .

The approximation that we will adopt in our formalism, which is supported by our present simulations and data from other groups [19, 20, 21], is to assume that the distribution function $P(\epsilon, \beta)$ is a Gaussian function with zero average

$$P(\epsilon, \beta) \propto \exp\left[-\frac{\epsilon^2}{2\sigma^2(\beta)}\right]. \quad (5)$$

The approximation of zero average is the reflection of the fact that no specific orientation of the solvent dipoles is created around a non-polar solute. This approximation is not necessarily always correct [9, 22, 23], but is insignificant for most of our development since a non-zero average, if it exists, can always be incorporated in a linear shift of ϵ . What is the most significant property for our analysis is the magnitude and the temperature dependence of the Gaussian width $\sigma^2(\beta)$.

Within the Gaussian approximation for the electrostatic fluctuations around a non-polar solute the thermodynamics of solvation gains a simple and physically transparent form. The chemical potential of solvation is

$$\mu_{0s} = -(\beta/2)\sigma^2(\beta). \quad (6)$$

In addition, one can determine the energy e and entropy s of electrostatic solvation

$$\begin{aligned} e &= \langle V_{0s} \rangle + \Delta e_{ss}, \\ Ts &= \frac{\langle V_{0s} \rangle}{2} + \Delta e_{ss}. \end{aligned} \quad (7)$$

In this equation, $\langle V_{0s} \rangle$ is the average solute-solvent electrostatic interaction energy when full solute-solvent interaction is turned on. From Eqs. (6) and (7),

$$\langle V_{0s} \rangle = -\beta\sigma^2(\beta). \quad (8)$$

The term Δe_{ss} in Eq. (7) determines the change in the interaction energy between the solvent molecules induced by electrostatic solute-solvent interaction. This energy term is identically equal to the corresponding contribution to the solvation entropy, $T\Delta s_{ss} = \Delta e_{ss}$, so that Δe_{ss} cancels out in the solvation chemical potential which is determined by solute-solvent interaction thermodynamics only [24, 25]. The term Δe_{ss} can be calculated by either taking the derivative of the Gaussian width $\sigma^2(\beta)$ or from a third-order correlation function

$$\Delta e_{ss} = -\frac{\beta^2}{2} \frac{\partial \sigma^2}{\partial \beta} = (\beta^2/2) \langle \delta V_{0s}^2 \delta H_0 \rangle_0. \quad (9)$$

In Eq. (9), the average $\langle \dots \rangle_0$ is over the ensemble of the non-polar solute in equilibrium with the solvent, collectively described by the Hamiltonian H_0 . In addition, $\delta V_{0s} = V_{0s} - \langle V_{0s} \rangle_0$ and $\delta H_0 = H_0 - \langle H_0 \rangle_0$ are deviations from the average values determined on the same unpolarized ensemble.

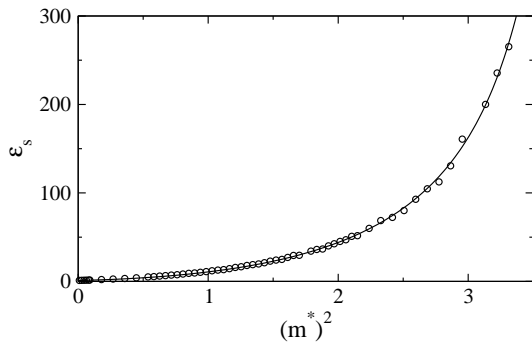


FIG. 1: Dielectric constant ϵ_s of the liquid of dipolar hard spheres vs the dipolar parameter $(m^*)^2 = \beta m^2/\sigma^3$; $\rho^* = 0.8$. The solid line represents the Padé approximation of the simulation data: $\epsilon_s(x) = (1 + a_1 x + a_2 x^2)/(1 + b_1 x + b_2 x^2)$ with $a_1 = 2.506$, $a_2 = 3.057$, $b_1 = -0.180$, $b_2 = -0.00865$ and $x = (m^*)^2$. The dielectric constants were calculated from NVT MC simulations of the homogeneous liquid of dipolar hard spheres using the Neumann [26] correction for the cutoff of dipolar interactions treated by the reaction-field formalism.

III. SIMULATIONS AND DATA ANALYSIS

While the equations presented in Sec. II are generally applicable to an arbitrary solute, we will use numerical Monte Carlo (MC) simulations [5] to determine the statistics of fluctuations produced in spherical cavities carved from a liquid of dipolar hard spheres (see Appendix for the description of the simulation protocol). The fluid of dipolar hard spheres leaves out many important properties of real liquids, most notably van der Waals forces and higher order multipoles. However, it allows a significant simplification of the solvation thermodynamics since all physical properties of the solvent are expressed in terms of only two parameters, the reduced density $\rho^* = \rho\sigma^3$ and the reduced dipole moment $(m^*)^2 = \beta m^2/\sigma^3$, where m is the dipole moment and σ is the diameter of the dipolar particles. Since the reduced density is fixed to $\rho^* = 0.8$ in our simulations, our results are fully defined in terms of two parameters: the reduced cavity radius R_0/σ and the polarity parameter $(m^*)^2$. The representation in terms of the dielectric constant ϵ_s can be easily achieved as well since these are well tabulated from our simulations as is shown in Fig. 1. The dielectric constants were calculated from Neumann's formalism [26] as described in detail in Ref. 27.

We will also limit our consideration to two types of electrostatic multipoles most commonly studied in theories and applications of solvation, point ion and point dipole [6, 7, 21]. In both cases, the corresponding multipole is placed at the center of the spherical cavity. The solute-solvent interaction potential is then given as $V_{0s} = q_0\phi_s$ in the case of the ion and $V_{0s} = -\mathbf{m}_0 \cdot \mathbf{E}_s$ for the dipole. In these relations, q_0 and m_0 are the charge and dipole moment of the probe multipole and ϕ_s and \mathbf{E}_s are, respectively, the potential and electric field produced by the solvent at the multipole position.

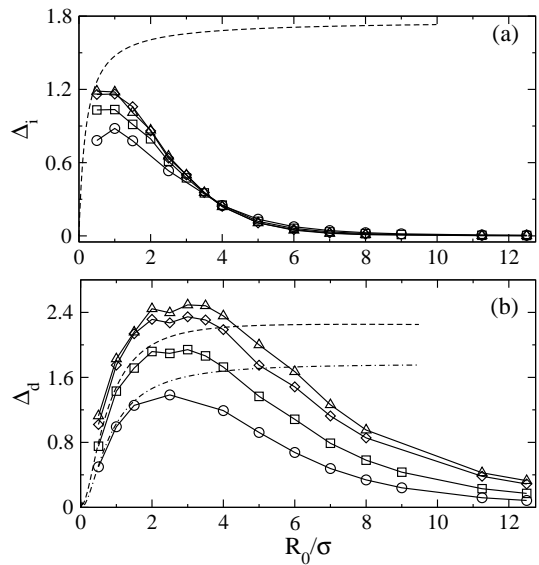


FIG. 2: Δ_i (a) and Δ_d (b) vs the cavity radius R_0 for $(m^*)^2 = 0.5$ (circles), 1.0 (squares), 2.0 (diamonds), and 3.0 (up-triangles). The dashed line in (a) gives the result of Eq. (17) for $m^* = 1.0$. The dash-dotted and dashed lines in (b) shows the application of Eq. (18) at $(m^*)^2 = 0.5$ and 1.0, respectively.

The main parameter entering the Gaussian model of solvation that we want to monitor is the Gaussian width $\sigma^2(\beta)$. Since we want to deal with dimensionless quantities, we will in fact calculate the temperature reduced parameter

$$\Gamma = \beta^2 \sigma^2(\beta) = \beta^2 \langle (\delta V_{0s})^2 \rangle_0. \quad (10)$$

Since this parameter depends on the multipolar character of the solute, it is convenient to take this information out and consider the parameter Δ such that the temperature-reduced electrostatic energy of the solute is taken out as a multiplier

$$\Gamma = w\Delta. \quad (11)$$

Here, the electric field of the multipole (charge or dipole) E_0 is used to define the electrostatic energy

$$w = (\beta/8\pi) \int_{\Omega} E_0(\mathbf{r})^2 d\mathbf{r}, \quad (12)$$

where the integral is taken over the solvent volume outside the spherical cavity.

The parameter w is equal to $\beta q_0^2/(2R_0)$ for an ion and $\beta m_0^2/(3R_0^3)$ for a dipole, where R_0 is the cavity radius. Therefore, one can calculate the parameter Δ according to the following relations in case on ion (subscript “i”) or dipolar (subscript “d”) solutes

$$\begin{aligned} \Delta_i &= 2\beta R_0 \langle (\delta\phi_s)^2 \rangle_0, \\ \Delta_d &= \beta R_0^3 \langle (\delta\mathbf{E}_s)^2 \rangle_0. \end{aligned} \quad (13)$$

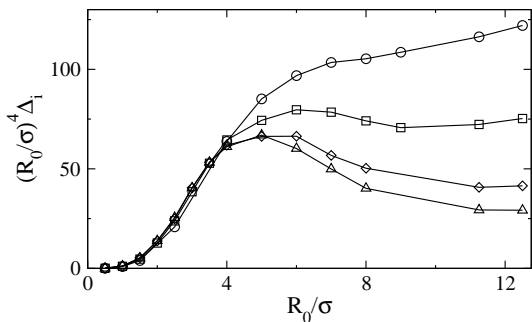


FIG. 3: $(R_0/\sigma)^4 \Delta_i$ vs the cavity radius R_0 for $(m^*)^2 = 0.5$ (circles), 1.0 (squares), 2.0 (diamonds), and 3.0 (up-triangles).

Similarly we will introduce the reduced parameter Δ_{ss} for the components of the internal energy and entropy arising from the alteration of the solvent-solvent interactions, $\beta \Delta \epsilon_{ss} = w \Delta_{ss}$:

$$\begin{aligned} \Delta_{ss}^i &= \beta^2 R_0 \langle (\delta \phi_s)^2 \delta H_0 \rangle_0, \\ \Delta_{ss}^d &= (\beta^2 R_0^3 / 2) \langle (\delta \mathbf{E}_s)^2 \delta H_0 \rangle_0. \end{aligned} \quad (14)$$

A few analytical results from standard electrostatics [3] can be used as benchmarks in calculating Δ_i and Δ_d . The continuum electrostatics of Born [6] and Onsager [7] equations gives the response functions $\Delta_{i,d}$ depending only on the dielectric constant ϵ_s of the dipolar liquid:

$$\Delta_i = 2 \left(1 - \frac{1}{\epsilon_s} \right) \quad (15)$$

and

$$\Delta_d = 6 \frac{\epsilon_s - 1}{2\epsilon_s + 1}. \quad (16)$$

In addition, several microscopic relations have been derived based on different formulations of the liquid-state theory. A closed-form equation for ion solvation is provided by the Ornstein-Zernike integral equations for the ion-dipole mixture solved in the mean-spherical approximation (MSA) [28]:

$$\Delta_i = \frac{2R_0}{R_0 + \Lambda_L} \left(1 - \frac{1}{\epsilon_s} \right). \quad (17)$$

In this equation, $\Lambda_L = 3\sigma\xi/(1 + 4\xi)$ is the correlation length of longitudinal polarization fluctuations of a dipolar liquid and ξ is the MSA polarity parameter [29].

An analogous MSA solution exists for the mixture of dipolar particles of different size [30] which gives the parameter Δ_d . Truncated perturbation expansions [31] are however known to work better in this case with the result [27, 32]

$$\Delta_d = 6 \left(\frac{R_0}{R_{\text{eff}}} \right)^3 \frac{y}{1 + \kappa(y, r_{0s}) y \sigma^3 I_{0s}^{(3)} / R_{\text{eff}}^3}. \quad (18)$$

Here, $r_{0s} = R_0/\sigma + 0.5$ is the reduced distance of the closest approach of the liquid molecules to the cavity and $y = (4\pi/9)\beta m^2 \rho$ is the standard density of dipoles in the dipolar liquid [4], ρ is the liquid number density. In addition, $I_{0s}^{(3)}(r_{0s}, \rho^*)$ is the three-particle perturbation integral which is a function of the liquid density and r_{0s} and $R_{\text{eff}}(r_{0s}, \rho^*)$ is the effective radius of the cavity

$$R_{\text{eff}}^{-3}(r_{0s}, \rho^*) = 3 \int_0^\infty \frac{dr}{r^4} g_{0s}^{(0)}(r). \quad (19)$$

In this equation $g_{0s}^{(0)}(r)$ is the hard-sphere distribution function of the liquid particles as a function of the distance r to the cavity center. All functions $R_{\text{eff}}(r_{0s}, \rho^*)$, $I_{0s}^{(3)}(r_{0s}, \rho^*)$, and $\kappa(y, r_{0s})$ are given as analytical functions of the corresponding parameters in Ref. 32.

IV. RESULTS

Our simulations have produced an unexpected result. We found that the scalings of electrostatic fluctuations and the corresponding chemical potentials with the cavity size do not follow the predictions of both the continuum electrostatics and microscopic solvation models in case of large cavities. The results are shown in Fig. 2. As is seen, the parameter Δ_i decays much faster than the expected $1/R_0$ scaling for all cavities greater than the size of the solvent particle. The large cavity scaling does not follow any universal law, but instead depends on the polarity (parameter m^*) of the liquid (Fig. 3). For the liquid polarities studied here, the large-cavity scaling of Δ_i is approximately $1/R_0^{4-6}$. Fluctuations of the electric field at the cavity center, representing dipole solvation, do not deviate that dramatically from the traditional expectations, but the parameter Δ_d still decays to zero instead of leveling off as suggested by Eqs. (15) and (18). In fact, Δ_d follows Eq. (18) quite well up to the cavity size about 4-5 times larger than the liquid particle, but then starts to drop following qualitatively the trend seen for the potential fluctuations. Continuum electrostatics [Eq. (15)] fails both qualitatively and quantitatively for electrostatic fluctuations of both the potential and the electric field.

There is a slight dependence of the variances on the number of particles in the simulation box. The variances extrapolated to $N \rightarrow \infty$ from simulations done at various system sizes are listed in Table I in the Appendix. This dependence does not affect any qualitative conclusions we make here. Since extrapolation to $N \rightarrow \infty$ creates a scatter of points, the results presented in Fig. 2 refer to a given system size only.

With the dramatic failure of some very basic expectations regarding electrostatic fluctuations, as is shown in Fig. 2, one wonders if the Gaussian approximation for the distribution of the electrostatic interaction energies fails for large cavities. We have tested this question by looking at the non-gaussianity parameter for both potential

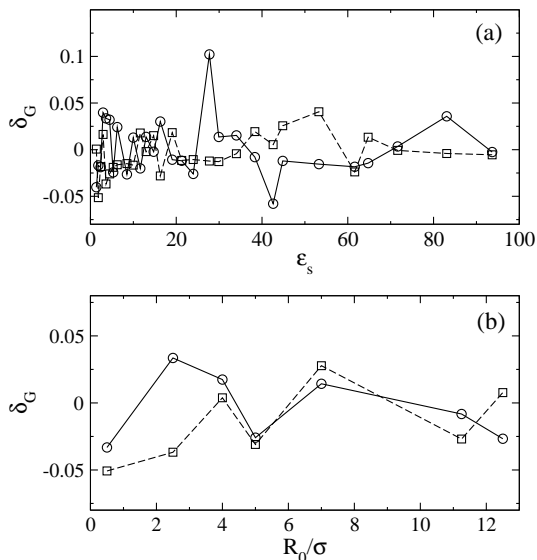


FIG. 4: Non-gaussianity parameter δ_G [Eq. (20)] vs ϵ_s (a) and R_0 (b). Points represent probe ions (circles) and probe dipoles (squares) for $R_0/\sigma = 2.5$ (a) and $(m^*)^2 = 0.5$ (b).

and field fluctuations:

$$\delta_G = \frac{\langle (\delta V_{0s})^4 \rangle_0}{\langle (\delta V_{0s})^2 \rangle_0^2} - 3. \quad (20)$$

This parameter was found to be around zero, as expected for the Gaussian noise, within about 5% of the simulation uncertainties (Fig. 4). The Gaussian approximation therefore seems reliable for our parameters database.

In order to gain more insight into the origin of our observations, we have calculated two local parameters related to the orientational and density structure of the liquid/cavity interface. Figure 5a shows the second-rank orientational order parameter of the permanent dipoles in the first solvation shell at the cavity surface:

$$p_2(r) = \left\langle \sum_j P_2(\hat{\mathbf{r}}_j \cdot \hat{\mathbf{e}}_j) \delta(\mathbf{r}_j - \mathbf{r}) \right\rangle. \quad (21)$$

Here, $P_2(x)$ is the second Legendre polynomial, $\hat{\mathbf{r}}_j = \mathbf{r}_j/r_j$ is the unit vector in the direction of the liquid particle j , and $\hat{\mathbf{e}}_j$ is the unit vector along its dipole moment. The orientational order parameter shown in Fig. 5a is calculated by limiting the distance r to liquid particles residing in the cavity's first solvation shell where it indicates the existence of a preferential orientational order. The first-rank orientational parameter, based on the first-order Legendre polynomial, is identically zero thus implying that there is no net dipolar polarization at the cavity surface. This result is distinct from the water surface where water's large quadrupole moment is responsible for asymmetry [9].

As the cavity gets larger the solvent dipoles find it more energetically favorable to orient parallel to the interface, as was also observed for 2D dipolar liquids [34],

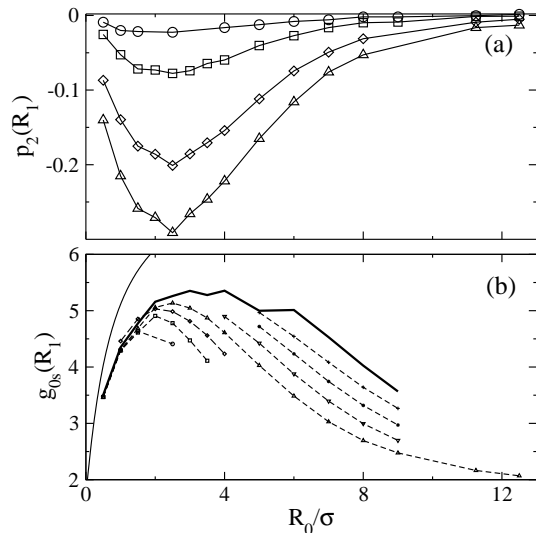


FIG. 5: (a): the orientational order parameter vs the cavity size for different polarities of the solvent, $(m^*)^2 = 0.5$ (circles), 1.0 (squares), 2.0 (diamonds), and 3.0 (up-triangles). (b): contact value of the radial distribution function at $R_1 = R_0 + \sigma/2$ vs the cavity radius. Shown are the results for different number of particles in the simulation box $N = 256$ (circles), 500 (squares), 864 (diamonds), 1372 (up-triangles), 2048 (down-triangles), 2916 (stars), 4000 (pluses). Extrapolation to $N \rightarrow \infty$ is shown by bold solid line. The dashed lines connect the points. The thin solid line gives the contact value of the distribution function in the hard-spheres mixture from Ref. 33.

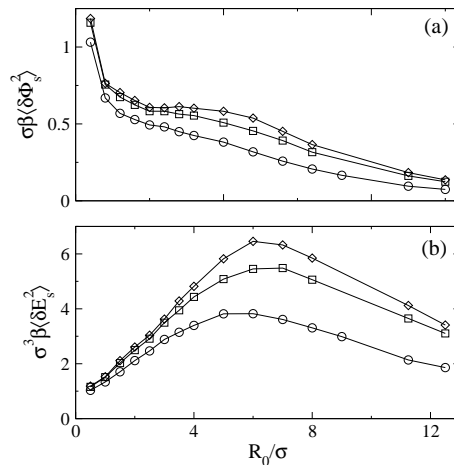


FIG. 6: $\sigma \beta \langle (\delta \phi_s)^2 \rangle$ (a) and $\sigma^3 \beta \langle (\delta \mathbf{E}_s)^2 \rangle$ (b) vs the cavity size for probe charge and dipole located the distance $\sigma/2$ from the cavity surface. The points refer to $(m^*)^2 = 1.0$ (circles), 2.0 (squares), and 3.0 (diamonds); $N = 1372$.

for water at cavity surfaces [35] and liquid-vapor interfaces [9], and for interfaces of dipolar liquids [36] from density-functional calculations. However, this preferential orientational order starts to dissolve with a further increase of the cavity size, after gaining maximum for the cavity about five times larger than the solvent particle.

This decay is related to the onset of softening of the first solvation shell indicated by the contact value of the pair cavity-solvent distribution function shown in Fig. 5b.

The contact value of the pair distribution function first rises as expected for a hard-sphere impurity in densely packed hard spheres [33] (solid line in Fig. 5b), but then starts to drop. This drop appears at approximately the same value $R_0/\sigma \simeq 2 - 2.5$ as both the downward turn of the orientational order parameter and the onset of deviation of the electric field fluctuations from the traditional predictions (Fig. 2). We therefore can conclude that the observed change in the character of the electrostatic fluctuations is related to softening of the liquid/cavity interface, which also loosens the energetic push for a specific dipolar order. We note, however, that the peak of the distribution function stays at the closest-approach value $R_1 = R_0 + \sigma/2$ and thus no dewetting [14] of the cavity interface occurs.

That the decay of the solvation energies is related to the softening of the interface is also seen from probing the fluctuations of the potential and field close to the cavity interface. Figure 6 shows the corresponding quantities for a point within the cavity kept one solvent radius $\sigma/2$ away from the interface once the cavity size is increased. Again, simple electrostatic arguments suggest that the solvation energetics should approach that for a probe charge or dipole next to an infinite dielectric wall. Depending on how the dielectric interface is defined, by the cavity boundary or by the distance of the closest approach, continuum electrostatics predicts [3] for $\sigma\beta\langle(\delta\phi_s)^2\rangle$ the value between $(\epsilon_s - 1)/(\epsilon_s + 1)$ and $0.5(\epsilon_s - 1)/(\epsilon_s + 1)$. The observed dependence does seem to inflect into a plateau at the level consistent with this prediction at intermediate cavity size, but then starts to decay. This decay is however much more gentle than in Fig. 2 indicating that the area next to the interface is effectively stronger solvating than the part of the hollow space closer to the cavity center.

The Gaussian approximation is a central part of our thermodynamic arguments and so we have done an additional test of its consistency also offering some deeper insights into the nature of electrostatic response functions. Since the chemical potential of solvation is given by the variance of the solute-solvent interaction potential [Eq. (6)], it becomes quadratic in a test multipole used to probe the electrostatic fluctuations. This result, known as the linear response approximation [21], suggests that the response function, obtained as the second derivative of μ_{0s} in the corresponding multipole, does not depend any more on the magnitude of that multipole. It also implies that $\Delta_{i,d}$ can be obtained from simulations of empty cavities but also from simulations involving actual multipoles inside the cavity. The chemical potential of solvation and corresponding parameters $\Delta_{i,d}$ are then calculated from the average solute-solvent interaction energy using Eq. (8). Since such simulations involving the probe charge are not straightforward due to the breakdown of the system neutrality and the related difficulty of

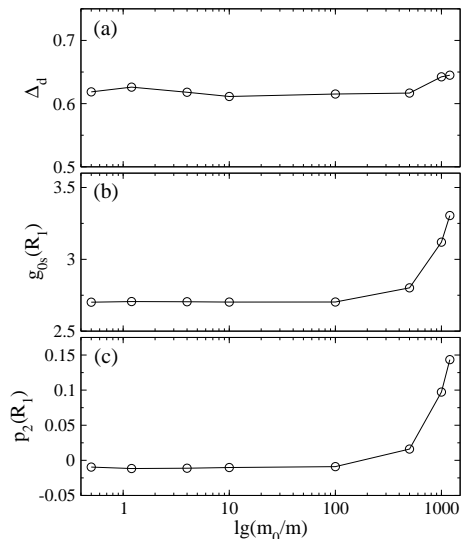


FIG. 7: Response function Δ_d (a), contact value of the cavity-solvent pair distribution function $g_{0s}(R_1)$ (b), and the orientational order parameter of the dipoles in the first solvation shell $p_2(R_1)$ (c) vs the magnitude of the solute dipole at the cavity center m_0 . Points are the results of MC simulations with $R_0/\sigma = 9.0$, $(m^*)^2 = 1.0$, and $N = 2048$. The lines connect the simulation points.

using the Ewald sums [37, 38], we have done simulations of point dipoles of varying magnitude placed at the cavity's center. The results are shown in Fig. 7 for the cavity size above the threshold seen in Fig. 2, $R_0/\sigma = 9.0$, and the simulation box containing $N = 2048$ solvent particles. There we show the parameter Δ_d calculated from $\langle V_{0s} \rangle$ at the varying magnitude of the solute dipole m_0 . Figures 7b and 7c also present the corresponding contact values of the cavity-solvent pair distribution function $g_{0s}(R_1)$ and the orientational order parameter $p_2(R_1)$. The response function Δ_d stays constant almost in the entire range of m_0 studied, starting to rise when the dipole inside the cavity exceeds the solvent dipole by three orders of magnitude. This rise is a reflection of the change in the microscopic structure of the interface as the first solvation shell gets stiffer under the pull of the solute dipolar field and the first-shell dipoles start to reorient along the field of the solute dipole. The observed changes in the functions $g_{0s}(R_1)$ and $p_2(R_1)$ are, however, much greater than the corresponding change in Δ_d testifying to the collective nature of the solvent dipolar response effectively depressing changes in the microscopic structure of the first solvation shell.

In Fig. 8 we show the same data as in Fig. 7, but obtained at a much smaller cavity size $R_0/\sigma = 1.5$. Here, the change in the local structure with increasing the solute dipole is more pronounced and Δ_d starts to show a dependence on the magnitude of the probe dipole signalling the appearance of nonlinear solvation effects. The variation in the response function is still mostly within 10% and can be accounted for by nonlinear extensions of

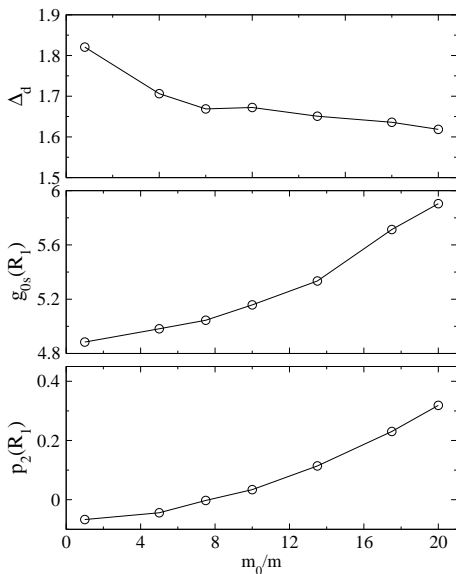


FIG. 8: Same as in Fig. 7 for $R_0/\sigma = 1.5$.

dipolar solvation models [27]. We need to stress, however, that the Gaussian approximation appears to be robust for large cavities which are of main interest for us here.

We next turn to the dependence of the cavity response functions on the liquid polarity. Figure 9a shows the dependence of Δ_i on the solvent dipole moment. For a small cavity size, when the standard scaling with the cavity size is expected to apply, the dependence of Δ_i on polarity does not show a saturation predicted by continuum electrostatics [Eq. (15)]. This saturation appears for a slightly larger cavity, but, as seen for a still larger cavity, it is simply en route to become a decreasing function of polarity for the largest cavities studied here. We can therefore conclude that there is no range of parameters where both the size scaling and the dependence on polarity predicted by the continuum electrostatics for the potential fluctuations are satisfied even at the qualitative level, not to mention the fact that the predicted values are significantly off.

The saturation predicted by the Onsager equation for dipole solvation [Eq. (16)] is never reached. In contrast to the potential fluctuations, the variance of the field is a uniformly increasing function with increasing solvent dipole for all cavity sizes studied here. A similar trend, for a narrower range of parameters, was previously observed by us [39] and it manifests itself in the solvation dynamics uniformly slower than continuum predictions [40]. The results for Δ_d from Eq. (18) are shown by the solid lines in Fig. 9b. As expected, there is a good agreement with the simulations for small cavities, but then the theory fails when the regime of solvation changes and Δ_d turns downward as in Fig. 2.

In Fig. 10 we show the results of calculations of the solvent-solvent component of the solvation entropy [Eq. (7)]. Within the Gaussian approximation, the ratio of

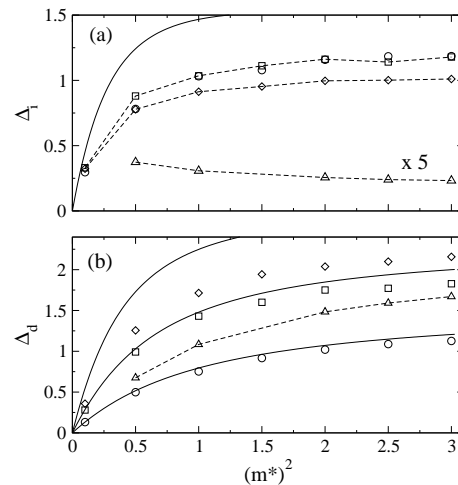


FIG. 9: Δ_i (a) and Δ_d (b) as functions of $(m^*)^2$ for $R_0/\sigma = 0.5$ (circles), 1.0 (squares), 1.5 (diamonds), and 6.0 (up-triangles). The solid line in (a) shows the result of using Eq. (17) at $R_0/\sigma = 1.0$. The solid lines in (b) show the result of Eq. (18) for $R_0/\sigma = 0.5, 1.0$, and 6.0 (from down up); the dashed lines in (a) and (b) connect the points. The data for Δ_i at $R_0/\sigma = 6.0$ (up-triangles) in (a) have been multiplied by a factor of 5 to bring them to the scale of the plot. The simulation points were obtained at $N = 1372$ dipolar hard spheres in the box.

the solvent-solvent component of the solvation entropy, $T_{s_{ss}} = \Delta e_{ss}$, and the solute-solvent component, $T_{s_{0s}} = -\beta\sigma^2(\beta)/2$, is given as the ratio of the corresponding reduced response functions

$$\chi_s = -\frac{s_{ss}^{i,d}}{s_{0s}^{i,d}} = \frac{2\Delta_{ss}^{i,d}}{\Delta_{i,d}}. \quad (22)$$

As is seen, for both the ionic and dipole solvation, there is a compensation between the ordering of the solvent by the solute, expressed by always negative s_{0s} , and the disordering of the solvent structure, expressed by positive s_{ss} . This compensation is however far from complete, in contrast to a much stronger compensation found for aqueous solvation [41]. The overall entropy of electrostatic solvation is therefore negative. Since the parameter χ_s in Eq. (22) depends weakly on the cavity size, the dramatic change in the character of solvation found here for $\sigma^2(\beta)$ will be reflected in both the enthalpy and entropy of electrostatic solvation which are often more accessible experimentally than solvation free energies. Very little is currently known about the magnitude of χ_s [42], in particular for large solutes. Our recent MD simulations of the redox entropy of metalloprotein plastocyanin [43] have produced $\chi_s \simeq 0.4$ ($R_0/\sigma \simeq 5.8$), although it is not clear if the Gaussian approximation is applicable to the protein electrostatics.

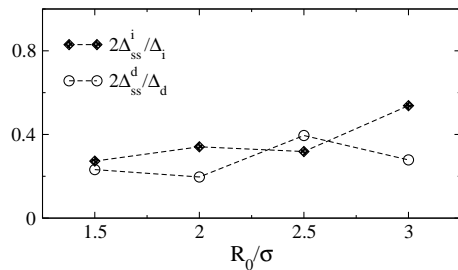


FIG. 10: The ratio of the solute-solvent and solvent-solvent components of the solvation entropy vs the cavity radius calculated for charge and dipole probe multipoles.

V. DISCUSSION

In this paper we have suggested to study polar solvation by using Eq. (3) which states that all the information required to calculate the solvation thermodynamics is contained in the distribution of electrostatic interaction energies around a fictitious solute with the solute-solvent electrostatic coupling switched off. This equation is exact and the approximation adopted here is that the distribution function $P(\epsilon)$ can be approximated by a Gaussian. The distribution $P(\epsilon)$ can generally be written as

$$P(\epsilon) \propto \exp[\beta\omega(\epsilon)] \quad (23)$$

and then the integral over ϵ in Eq. (3) can be taken by the steepest descent around the stationary point ϵ_0 defined by the condition $\omega'(\epsilon_0) = 1$. The Gaussian approximation is then equivalent to assuming all the terms except the linear one can be dropped from the series expansion of $\omega'(\epsilon)$ in powers of $(\epsilon - \epsilon_0)$.

Our simulations have not identified any significant deviations from non-gaussianity. Extensive simulations done with ionic and dipolar solutes over the last decades [19, 20, 21, 39] have also resulted in the conclusion that the Gaussian picture is an accurate one implying that $P(\epsilon)$ is globally a Gaussian function. However, one can argue that we could not sample sufficiently around ϵ_0 and thus cannot assess the deviations from Gaussianity. While that might be true for strong solute-solvent interactions, for which a significant data-base pointing otherwise exists [39], energy ϵ_0 is expected to decrease with increasing the cavity size and the Gaussian approximation is expected to become increasingly accurate (as indeed seen from comparing Figs. 7 and 8). However, it is in this range of large cavities, almost completely neglected in previous studies of electrostatic solvation, that we found the most dramatic deviations from the traditional expectations.

The main finding of this study is that electrostatic solvation by polar liquids changes its regime at the size of the cavity about 4-5 times larger than the size of the solvent particle. The regime of small cavities can be reasonably understood with molecular solvation models and in particular the results for the electric field fluctuations

(probe dipole) are in a very good quantitative agreement with the results of perturbation solvation models. The regime of large cavities is dramatically different and cannot be described by the models traditionally employed for solvation problems.

What we have observed here is a dramatic decay of the solvation strength in the middle of the cavity, much faster than expected from both the continuum electrostatics and microscopic solvation models. For instance, the variance of the electrostatic potential decays as $1/R_0^{4-6}$ instead of the expected $1/R_0$ scaling. The core of a growing hollow cavity thus becomes non-polar much faster than previously anticipated. What it practically means is that there is very little solvation stabilization for charges inside a large mesoscale object. This might be a reason why natural systems requiring hydration of large molecular assemblies (proteins, etc.) rely on solvation of surface charges for which much slower decay of solvating power due to softening of the interface was found here. In application to the problem of protein folding, this observation implies a very strong driving force for placing ionized residues and cofactors stabilizing protein solvation closer to the interface.

Acknowledgments

This research was supported by the National Science Foundation (CHE-0616646). CPU time for parallel MC simulations was provided by ASU's Center for High Performance Computing.

APPENDIX A: SIMULATION PROTOCOL AND RESULTS

MC simulations were performed with the standard NVT Metropolis algorithm. The initial configuration was constructed starting from an *fcc* lattice of liquid hard-spheres of diameter σ and density $\rho^* = 0.8$. The hard-sphere solute/cavity was then “grown” in the center of the simulation box by increasing the initial cavity diameter of 0.5σ with 0.002σ increment, adjusting σ to ensure constant density, and moving the solvent particles according to the Metropolis algorithm. After the solute/cavity was constructed, the initial configuration was created from $10^5 - 10^6$ parallel steps (using OpenMPI) producing different initial configurations for each processor. The subsequent runs were then carried out on each processor separately thus minimizing interprocessor communications. To guarantee the Markovian statistics, the random number generators used in the MC moves were seeded independently between the processors. This implementation has resulted in a linear scaling of the program output with the number of processors. The production runs of $(1 - 5) \times 10^6$ steps were performed on 10 processors per $(m^*)^2$ per cavity size.

The simulation protocol employed the minimum image convention and the reaction-field correction [5] for the cut-off of dipolar interactions at one-half of the cubic simulation box. Ewald sums [37] were also tested and gave results identical within simulation uncertainties. The reaction-field correction was preferred due to better performance. The dependence on the simulation box size was carefully checked in particular since growing

cavity required larger number of liquid particles to eliminate finite-size effects. The number of particles N was varied in the range $N = 108, 256, 500, 864, 1372, 2048, 2916,$ and 4000 depending on the cavity size. The representative results for Δ_i and Δ_d listed in Table I were obtained by averaging over several simulation runs with different box sizes and also by extrapolating the plots of corresponding values vs $1/N$ to the $N \rightarrow \infty$ limit.

-
- [1] T. L. Beck, M. E. Paulaitis, and L. R. Pratt, *The potential distribution theorem and models of molecular solutions* (Cambridge University Press, Cambridge, 2006).
- [2] J. P. Hansen and I. R. McDonald, *Theory of Simple Liquids* (Academic Press, Amsterdam, 2003).
- [3] L. D. Landau and E. M. Lifshitz, *Electrodynamics of continuous media* (Pergamon, Oxford, 1984).
- [4] C. J. F. Böttcher, *Theory of Electric Polarization*, vol. 1 (Elsevier, Amsterdam, 1973).
- [5] M. P. Allen and D. J. Tildesley, *Computer Simulation of Liquids* (Clarendon Press, Oxford, 1996).
- [6] M. Born, *Z. Phys.* **1**, 45 (1920).
- [7] L. Onsager, *J. Am. Chem. Soc.* **58**, 1486 (1936).
- [8] A. V. Marenich, C. J. Cramer, and D. G. Truhlar, *J. Chem. Theory Computat.* **4**, 877 (2008).
- [9] V. P. Sokhan and D. J. Tildesley, *Mol. Phys.* **92**, 625 (1997).
- [10] D. R. Martin and D. V. Matyushov, *Europhys. Lett.* **82**, 16003 (2008).
- [11] D. Chandler, *Nature* **437**, 640 (2005).
- [12] A. A. Rashin, *Prog. Biophys. Molec. Biol.* **60**, 73 (1993).
- [13] K. Lum, D. Chandler, and J. Weeks, *J. Phys. Chem. B* **103**, 4570 (1999).
- [14] G. Hummer and S. Garde, *Phys. Rev. Lett.* **80**, 4193 (1998).
- [15] D. M. Huang and D. Chandler, *Phys. Rev. E* **61**, 1501 (2000).
- [16] H. S. Ashbaugh and L. R. Pratt, *Rev. Mod. Phys.* **78**, 159 (2006).
- [17] A. C. Maggs and R. Everaers, *Phys. Rev. Lett.* **96**, 230603 (2006).
- [18] T. Rudas, C. Schröder, and O. Steinhauser, *J. Chem. Phys.* **124**, 234908 (2006).
- [19] R. A. Kuharski, J. S. Bader, D. Chandler, M. Sprik, M. L. Klein, and R. W. Impey, *J. Chem. Phys.* **89**, 3248 (1988).
- [20] J. Blumberger and M. Sprik, *J. Phys. Chem. B* **109**, 6793 (2005).
- [21] J. Aqvist and T. Hansson, *J. Phys. Chem.* **100**, 9512 (1996).
- [22] H. S. Ashbaugh, *J. Phys. Chem. B* **104**, 7235 (2000).
- [23] D. S. Cerutti, N. A. Baker, and J. A. McCammon, *J. Chem. Phys.* **127**, 155101 (2007).
- [24] H.-A. Yu and M. Karplus, *J. Chem. Phys.* **89**, 2366 (1988).
- [25] D. Ben-Amotz, F. O. Raineri, and G. Stell, *J. Phys. Chem. B* **109**, 6866 (2005).
- [26] M. Neumann, *Mol. Phys.* **57**, 97 (1986).
- [27] D. V. Matyushov and B. M. Ladanyi, *J. Chem. Phys.* **110**, 994 (1999).
- [28] D. Y. C. Chan, D. J. Mitchell, and B. W. Ninham, *J. Chem. Phys.* **70**, 2946 (1979).
- [29] M. S. Wertheim, *J. Chem. Phys.* **55**, 4291 (1971).
- [30] B. C. Freasier and D. J. Isbister, *Mol. Phys.* **38**, 81 (1979).
- [31] B. Larsen, J. C. Rasaiah, and G. Stell, *Mol. Phys.* **33**, 987 (1977).
- [32] S. Gupta and D. V. Matyushov, *J. Phys. Chem. A* **108**, 2087 (2004).
- [33] D. V. Matyushov and B. M. Ladanyi, *J. Chem. Phys.* **107**, 5815 (1997).
- [34] J. J. Weis, *Mol. Phys.* **100**, 579 (2002).
- [35] S. Rajamani, T. Ghosh, and S. Garde, *J. Chem. Phys.* **120**, 4457 (2004).
- [36] P. Frodl and S. Dietrich, *Phys. Rev. A* **45**, 7330 (1992).
- [37] S. W. DeLeeuw, J. W. Perram, and E. R. Smith, *Proc. R. Soc. London Ser. A* **373**, 27 (1980).
- [38] G. Hummer, L. R. Pratt, and A. E. Garcia, *J. Phys. Chem. A* **102**, 7885 (1998).
- [39] A. Milischuk and D. V. Matyushov, *J. Phys. Chem. A* **106**, 2146 (2002).
- [40] D. V. Matyushov, *J. Chem. Phys.* **122**, 044502 (2005).
- [41] P. K. Ghorai and D. V. Matyushov, *J. Phys. Chem. A* **110**, 8857 (2006).
- [42] D. Ben-Amotz and R. Underwood, *Acc. Chem. Res.* p. to be published (2008).
- [43] D. N. LeBard and D. V. Matyushov, *J. Chem. Phys.* **128**, 155106 (2008).

TABLE I: Values of Δ_i and Δ_d for $(m^*)^2 = 0.5, 1.0, 2.0, 3.0$, $\epsilon = 3.63, 8.51, 29.9, 93.7$, respectively. Extrapolations (ext.) were done with $N = 108, 256, 500, 864, 1372, 2048, 2916, 4000$ data when available, linearly fitting $\Delta_{i,d}$ vs. $1/N$ and taking the intercept. The system sizes used for the extrapolations are given in the footnotes.

R_0/σ	N	$(m^*)^2$							
		0.5		1.0		2.0		3.0	
		Δ_i	Δ_d	Δ_i	Δ_d	Δ_i	Δ_d	Δ_i	Δ_d
0.5	1372	0.781	0.498	1.031	0.753	1.158	1.020	1.185	1.126
	ext. ^a	0.814	0.572	1.052	0.761	1.210	1.030	1.265	1.153
1.0	1372	0.892	1.001	1.035	1.431	1.184	1.801	1.240	1.939
	ext. ^b	0.863	1.009	1.050	1.449	1.171	1.768	1.198	1.854
1.5	1372	0.778	1.256	0.936	1.760	1.058	2.137	1.073	2.286
	ext. ^c	0.834	1.292	1.011	1.772	1.084	2.112	1.103	2.238
2.0	1372	–	–	0.795	1.918	0.859	2.314	0.866	2.444
	ext. ^c	–	–	0.862	1.965	0.844	2.300	0.859	2.394
2.5	1372	0.533	1.384	0.632	1.955	0.670	2.365	0.666	2.513
	ext. ^c	0.619	1.491	0.692	2.079	0.695	2.470	0.710	2.627
3.0	1372	–	–	0.475	1.941	0.499	2.345	0.499	2.492
	ext. ^d	–	–	0.612	2.122	0.550	2.468	0.556	2.587
3.5	1372	–	–	0.352	1.864	0.355	2.307	0.355	2.482
	ext. ^d	–	–	0.459	2.129	0.376	2.539	0.375	2.578
4.0	1372	0.249	1.191	0.252	1.723	0.242	2.188	0.239	2.356
	ext. ^e	–	–	0.495	2.186	0.528	2.597	0.533	2.699
5.0	1372	0.136	0.927	0.124	1.431	0.112	1.830	0.107	2.000
	ext. ^f	0.299	1.393	0.310	2.004	0.251	2.388	0.246	2.556
6.0	1372	0.075	0.675	0.061	1.084	0.051	1.483	0.046	1.670
	ext. ^g	0.298	1.449	0.296	2.061	0.236	2.484	0.233	2.553
7.0	1372	0.043	0.478	0.033	0.789	0.024	1.124	0.021	1.263
	ext. ^g	0.192	1.233	0.183	1.834	0.133	2.203	0.125	2.373
8.0	1372	0.026	0.338	0.018	0.581	0.012	0.855	0.010	0.952
	ext. ^g	0.128	1.003	0.114	1.540	0.054	1.790	0.048	2.004
9.0	1372	0.017	0.241	0.011	0.433	–	–	–	–
	ext. ^g	0.087	0.803	0.071	1.258	–	–	–	–
10.0	4000	–	–	0.036	0.830	0.029	1.176	0.025	1.304
11.25	1372	0.0073	0.119	0.0045	0.230	0.0025	0.383	0.0018	0.426
12.5	1372	0.0050	0.085	0.0031	0.172	0.0017	0.287	0.0012	0.329

^a108, 256, 500, 1372, 2048

^b108, 256, 500, 864, 1372

^c256, 500, 864, 1372

^d500, 864, 1372

^e864, 1372, 2048

^f500, 864, 1372, 2048, 2916, 4000

^g1372, 2048, 2916, 4000